



A modeling study by artificial neural network on ethidium bromide adsorption optimization using natural pumice and iron-coated pumice

Behzad Heibati^{a,b}, Susana Rodriguez-Couto^{c,d}, Okan Ozgonenel^e,
Nurdan Gamze Turan^f, Annalisa Aluigi^g, Mohammad Ali Zazouli^h,
Mohammad Ghanbari Ghoskhal^{b,i}, Mahmoud Mohammadyan^{a,*}, Ahmad B. Albadarin^{j,*}

^aFaculty of Health and Health Sciences Research Center, Department of Occupational Health Engineering, Mazandaran University of Medical Sciences, Sari, Iran, emails: bheibati@gmail.com (B. Heibati), Mohammadyan@yahoo.com (M. Mohammadyan)

^bDepartment of Environmental Health Engineering, School of Public Health, Tehran University of Medical Sciences, Tehran, Iran, email: ghanbarym@yahoo.com (M.G. Ghoskhal)

^cCEIT, Unit of Environmental Engineering, Paseo Manuel de Lardizabal 15, San Sebastian 20018, Spain, email: srodriguez@ceit.es

^dIKERBASQUE, Basque Foundation for Science, Alameda de Urquijo 36, Bilbao 48011, Spain

^eElectrical & Electronic Engineering Department, Ondokuz Mayıs University, Samsun 55139, Turkey, email: okanoz@omu.edu.tr

^fEnvironmental Engineering Department, Ondokuz Mayıs University, Samsun 55139, Turkey, email: gturan@omu.edu.tr

^gCNR-ISOF (National Research Council—Institute of Organic Chemistry and Photoreactivity), via P. Gobetti 101, Bologna 40129, Italy, email: annalisa.aluigi@isof.cnr.it

^hFaculty of Health and Health Sciences Research Center, Department of Environmental Health Engineering, Mazandaran University of Medical Sciences, Sari, Iran, email: zazoli49@yahoo.com

ⁱPhD Student of Environmental Health Engineering, Department of Environmental Health Engineering, School of Public Health, Tehran University of Medical Sciences, Tehran, Iran

^jDepartment of Chemical and Environmental Sciences, University of Limerick, Limerick, Ireland, Tel. +44 74 6080 5982;

Fax: +353 0 61 202568; email: Ahmad.B.Albadarin@ul.ie

Received 3 February 2015; Accepted 1 June 2015

ABSTRACT

In this study, the potential of natural pumice (NP) and iron-coated pumice stone (Fe-CP) as novel low-cost adsorbents to remove ethidium bromide (EtBr) from aqueous solutions was investigated. The operational parameters affecting removal efficiency and adsorption capacity such as adsorbent dose, initial EtBr concentration, pH, and contact time were studied in order to maximize EtBr removal. The maximum amount of adsorbed EtBr (q_m) using NP and Fe-CP was 40.25 and 45.08 mg g⁻¹, respectively. It was found that EtBr adsorption followed the Freundlich isotherm model and fitted the pseudo-second-order kinetics equation for both adsorbents. In addition, the experimental system could be easily modeled by artificial neural network calculations.

Keywords: Artificial neural network (ANN); Ethidium bromide (Etbr); Pumice; Iron-coated pumice; Adsorption isotherms; Kinetics studies

*Corresponding authors.

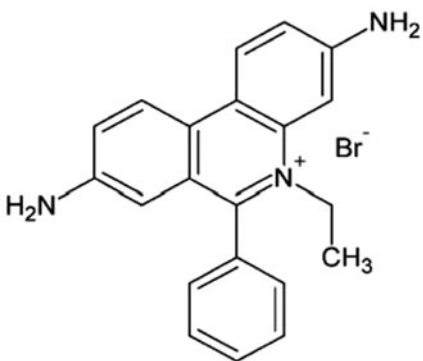
1. Introduction

Ethidium bromide (3,8-diamino-6-phenyl-5-ethylphenanthridinium bromide, 2,7-diamino-10-ethyl-9-phenylphenanthridinium bromide; homidium bromide; Dromilac; EtBr) is a dark red, crystalline compound, soluble in water, whose molecular structure and physicochemical properties are shown in Table 1 [1,2]. EtBr is widely used in research laboratories as a stain and a nonradioactive marker for rapid visualization of nucleic acids bands in electrophoresis gels and in other methods of gel-based nucleic acid separation [3]. EtBr is recognized as a toxic and hazardous waste due to its potent mutagenous and teratogenous effects. For the aforementioned reason, careful handling and disposal procedures are required [4]. Nowadays, different methods are used to remove dyes and organic compounds from aqueous solutions such as chemical and electrochemical degradation [2], photocatalytic degradation [5,6], incineration, biological treatments, and adsorption [7,8]. Chemical degradation of EtBr is complicated and requires the use of expensive reagents, which increases the price of wastewater treatment. Also, biological methods are ineffective in removing EtBr because of its resistance to biodegradation. Among the available methods, the adsorption process has been shown to be the most suitable method for EtBr removal from aqueous solutions [9]. Thus, a variety of natural and synthetic materials have been tested as EtBr adsorbents, such as XAD 7 resin [10] and single-walled nanotubes [11]. However, commercially activated carbon and nanotubes are expensive and need to be regenerated continuously in order to reduce the processing cost. Therefore, the development of efficient and low-cost materials to remove EtBr from aqueous solutions is needed. Considering the difference in adsorption capacity, cost, and availability of different adsorbents, the

applicability of regional adsorbents deserves attention. Pumice is a volcanic rock coming from solidified volcanic lava and can be found in many places worldwide. In particular, in Iran, this rock can be abundantly found in many parts, especially in Azerbaijan. Pumice has high porosity and low weight where it normally either floats on water or sinks slowly. Pumice rocks are porous and amorphous materials which consist mainly of SiO₂ and Al₂O₃. Traditionally, pumice has been used in the construction industry [12–14]. In recent years, pumice has also been used in the field of water and wastewater treatment, both in natural and modified forms, to remove fluoride [15], azo dyes [16], phenol and 4-chlorophenol [17], heavy metals [18], SO₂ [19], and natural organic matter [20]. In order to improve the adsorption capacity of naturally occurring pumice, various organic and inorganic chemicals such as hydroxy-aluminum [21], hydroxy-iron salts and magnesium chloride [12], and hydrogen peroxide [14] have been used.

Artificial neural networks (ANNs) have been widely used to solve environmental problems because of their reliable, robust, and salient characteristics in capturing the nonlinear relationships existing between variables (multi-input/output) in complex systems [22]. This approach is particularly useful in applications where the complexity of the mechanisms underlying process performance is high; this is the case of biological treatment processes for pollution control. Therefore, ANNs have gained increasing consideration in wastewater treatment modeling and control [23]. Thus, recently, Turan et al. used hazelnut shells as a new adsorbent to remove Zn(II) from leachate and proposed a feed-forward three-layer network type. Among many ANN structures, the multi-layer back-propagation network is by far the

Table 1
The molecular structure and physicochemical properties of EtBr

	Molecular formula	C ₂₁ H ₂₀ BrN ₃
	Molar mass	394.29 g mol ⁻¹
	Appearance	Purple-red solid
	Meltingpoint	260–262°C
	Solubility in water	40 g L ⁻¹
	λ _{max}	480 nm

most popular [23,24]. The ability to identify a relationship from given input vectors make it possible for ANNs to solve large-scale complex engineering problems such as pattern recognition, classification, nonlinear modeling, association, and control [25]. A neural network is characterized by its architecture that represents the pattern of association between nodes, its method of determining, the connection weights, and the activation function. ANNs are classified according to the number of layers in either single or multi-layer and based on the direction of the information in stream and feed-forward processing. The input variables determine the number of input nodes in the input layer. The output layer is where the output is processed and sent to an external source. The number of hidden layer nodes in the hidden layer is determined by a trial and error procedure until the error is minimized. The number of neurons in the hidden layer determines the performance of a network. Therefore, too few or too many nodes in the hidden layer lead to poor performance of the network. It is recommended that the total number of hidden layer nodes is at least three times of the total number of input layer nodes in order to avoid failure to reach convergence [26]. Due to the number of advantages of pumice stone, the aim of the present work was to investigate its applicability to remove EtBr from aqueous solutions. For this, the effect of pH, adsorbent dose, initial EtBr concentration, and contact time on the adsorption process was studied. On the basis of batch adsorption experiments, a three-layer ANN model to predict the EtBr removal efficiency of pumice adsorbents was applied. The adsorption of EtBr from aqueous solutions was optimized to determine the optimal network structure. The use of ANN based on radial basis functions (RBF) was also investigated and proposed as an efficient network type for adsorption studies.

2. Material and methods

2.1. Preparation of iron-coated pumice (Fe-CP)

Natural pumice (NP) stone was obtained from Tikmeh Dash region of eastern Azerbaijan (Iran). Prior to the coating of the surface of the pumice stone with iron, the NP was washed several times with double distilled water and then immersed in 1 N HCl for 24 h. After that the pumice was rinsed several times by double distilled water until its effluent turbidity reached at least 0.1 NTU (Nephelometric Turbidity Unit). Finally, the prepared sample was crushed and sieved to 20 meshes for experimental studies. The crushed and sieved particles of pumice were

immersed in double distilled water for 24 h and then dried in an oven at 105°C for 14 h. In order to coat the particles with iron, 50 g of pumice particles and 150 mL of 0.1 M $\text{Fe}(\text{NO}_3)_3 \cdot 9\text{H}_2\text{O}$ solution were placed into a beaker and the pH was adjusted to 11 by adding 10 M NaOH solution dropwise while stirring for 2 min. Thereafter, the beaker was kept in a static and stable state at laboratory temperature ($24 \pm 1^\circ\text{C}$) for 72 h, and then, the coated pumice was dried in an oven at 110°C for 24 h. In order to remove traces of unbounded iron, the dried particles were washed again with double distilled water and dried in an oven at 105°C for 14 h [13]. The chemical structure of the adsorbents was determined by X-ray fluorescence (Model XRert, Holland). In addition, the morphology of the pumice before and after coating was characterized by scanning electron microscopy (SEM) (XL30, Philips). The specific areas of the raw and iron-coated pumice have been previously determined as 2.34 and 3.00 m^2/g , respectively [12,27].

2.2. Experimental

Batch adsorption studies were performed in 100-mL Erlenmeyer flasks under magnetic stirring conditions at room temperature ($24 \pm 1^\circ\text{C}$). A stock solution ($1,000 \text{ mg L}^{-1}$) of EtBr was prepared in deionized water and kept at room temperature ($24 \pm 1^\circ\text{C}$). Required concentrations of EtBr standards were prepared by appropriate dilution of the above EtBr stock solution. The adsorption processes were conducted by mixing 4 g of NP or 4 g of Fe-CP, according to the experiment, in 100-mL Erlenmeyer flasks containing 50 mL of aqueous solutions with different concentrations of EtBr. The flasks were kept at room temperature ($24 \pm 1^\circ\text{C}$) under shaking (120 rpm). The effect of pH (from 3 to 10), initial EtBr concentration (from 10 to 100 mg L^{-1}), adsorbent dose (from 1 to 10 g L^{-1}), and contact time (from 1 to 210 min) on the adsorption process was studied. After the adsorption process, the samples were filtered and analyzed for EtBr concentration.

The amount of EtBr adsorbed onto the adsorbent, q_t (mg g^{-1}) was calculated as follows:

$$q_t = \frac{(C_0 - C_t) \times V}{m} \quad (1)$$

where C_0 (mg L^{-1}) and C_t (mg L^{-1}) are the initial concentration of EtBr and the EtBr concentration after a particular adsorption time t , respectively, m (g) the mass of the adsorbent, and V (L) the volume of the liquid phase.

2.3. Analysis

The surface morphology and the related chemical composition of the adsorbents were analyzed by SEM and energy dispersive X-ray diffraction (EDX), respectively. A colorimetric method was used to analyze the EtBr concentration of the samples. Thus, EtBr was measured at a wavelength of 480 nm using a UV–vis spectrophotometer according to the method presented in standard methods for the examination of water and wastewater [28]. Statistical analyses were performed using Excel software.

2.4. Modeling approach

In this work, Matlab™ was used to predict the adsorption efficiency. A three-layer ANN, an input layer with 2 neurons (initial pH, adsorbent dosage, contact time, and initial EtBr concentration), a hidden layer with 2 neurons, and an output layer with 1 neuron (2-2-1 and 1-2-1) were established. Six training algorithms were tested according to their performance in order to select the best back-propagation (BP) training algorithm. Following benchmark comparisons, an optimization was carried out for the best BP algorithm. Then, the three-layer ANN was evaluated by the best BP algorithm. Finally, the use of an ANN based on RBF was also investigated and compared with the classical feed-forward BP neural networks.

3. Results and discussion

3.1. Adsorbent characteristics

The solid structure and photomicrography of the exterior surface of the NP and Fe-CP analyzed by SEM are shown in Fig. 1. The SEM images of NP and Fe-CP in Fig. 1 showed ordered silica crystals at their surface, and micropores or roughness with small cracks on the NP surface. The Fe-CP (Fig. 1(b)) had a significant rougher surface than the NP (Fig. 1(a)). The results of EDX analysis are shown in Fig. 1(c) and (d) and summarized in Table 2. Fig. 1(c) and (d) indicates that the major constituents of the adsorbents included Fe, Si, and K, while other elements were present in relatively small amounts. The chemical composition on the Fe-CP surface was different from that of the original pumice; after the coating, the presence of Fe was observed to increase from 16.63 to 51.33%.

3.2. Kinetics studies

As can be seen in Fig. 2, the removal efficiency increased with time (for an EtBr initial concentration

of 30 and 100 mg L⁻¹, an adsorbent dose of 4 g L⁻¹ and pH 10) until reaching a constant value after 90 and 150 min for NP and Fe-CP, respectively, corresponding to the saturation of the adsorbent. The removal of EtBr was found to be rapid during the initial period of contact time, and then, it diminished with the increase in contact time. This was probably due to the abundant number of free active sites on the adsorbents at the beginning of the process, whereas with the gradually increased occupancy of these sites with time, the adsorption process becomes less efficient [29].

Kinetics modeling not only allows estimation of adsorption rates but also leads to suitable rate expressions characteristic of possible reaction mechanisms. In this respect, three kinetic models including the pseudo-first-order equation (Eq. (2)), pseudo-second-order equation (Eq. (3)), and intra-particle diffusion (Eq. (4)) [30–32] were tested.

The pseudo-first-order rate expression is given as follows:

$$q_t = q_e(1 - e^{-k_1 t}) \quad (2)$$

where q_e is the adsorption capacity of the adsorbate (mg g⁻¹) at equilibrium and k_1 is the pseudo-first-order rate constant.

Pseudo-second-order kinetics is expressed as follows:

$$q_t = \frac{k_2 q_e^2}{(1 + k_2 q_e t)} t \quad (3)$$

where k_2 is the pseudo-second-order rate constant (g mg⁻¹ min⁻¹).

These equations have been widely used to describe adsorption kinetics data. The most accurate model was considered to be based on the regression coefficient (R^2) and the comparison of the q_e values to the experimental ones. Kinetics of dye removal is shown in Fig. 2 and the corresponding parameters are given in Table 3. As shown, the kinetics of EtBr removal by both NP and Fe-CP followed the pseudo-second-order equation. Additionally, the calculated values of q_e were close to the experimental ones while the q_e values calculated from the pseudo-first-order kinetic equation were underestimated as it was revealed above. Accordingly, the pseudo-second-order kinetic model could be used to successfully calculate the amount of EtBr adsorbed at equilibrium using the kinetic experimental results. These results suggested that the pseudo-second-order adsorption mechanism was predominant and adsorption was controlled by

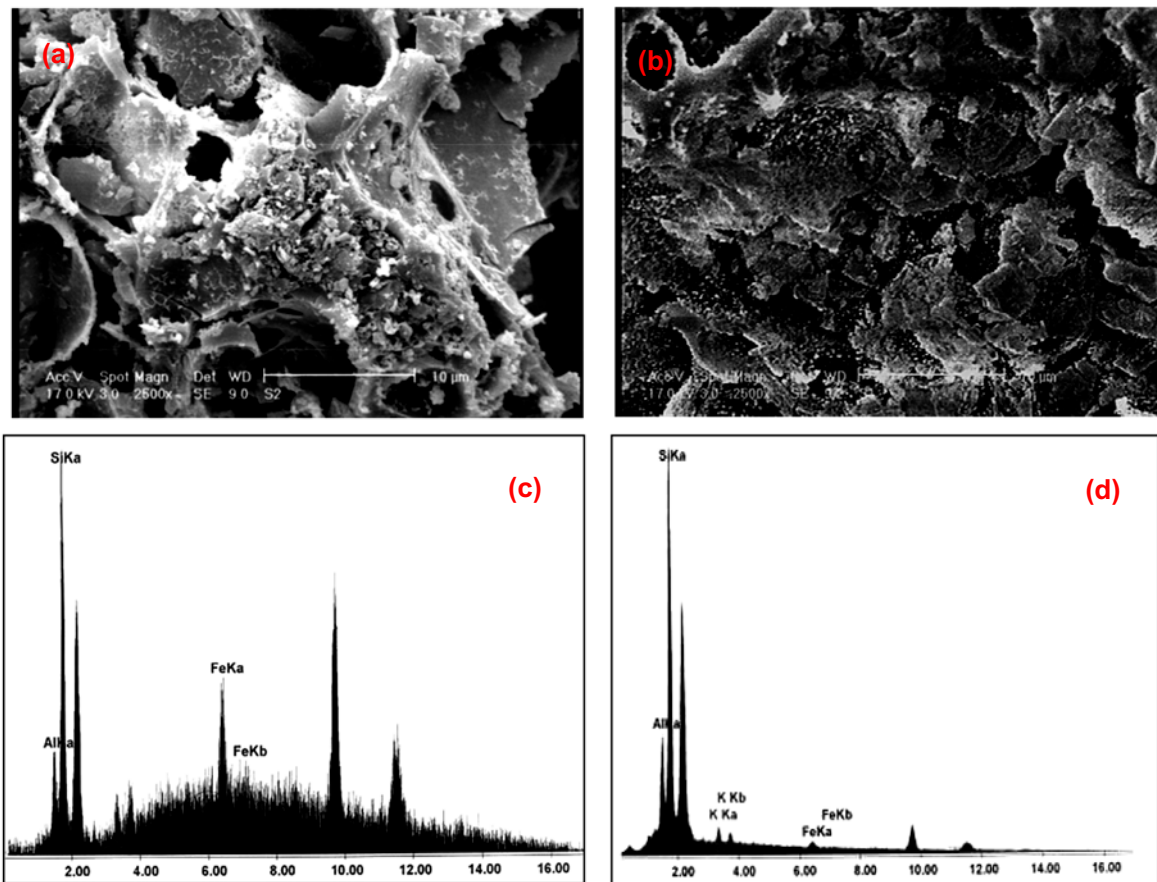


Fig. 1. (a) SEM image of the NP; (b) SEM image of the iron-coated pumice (Fe-CP); (c) X-ray diffraction spectrum (XRD) of the NP; (d) XRD of the Fe-CP.

Table 2
Elemental composition (wt.%) of NP and iron-coated pumice (Fe-CP) obtained from EDX characterization

Elements	Al	Si	K	Fe
NP	13.55	63.81	6.021	16.63
ICP	9.104	39.53	–	51.33

the chemisorption process [13]. In addition, the intraparticle diffusion model is a commonly used technique for identifying the mechanism involved in the adsorption process. This was studied by plotting EtBr adsorption, q_t , vs. the square root of the time, $t^{1/2}$, as shown in Fig. 2. The rate parameter of intraparticle diffusion can be defined as follows:

$$q_t = k_{ip} \times t^{1/2} \quad (4)$$

where k_{ip} is the intraparticle diffusion rate constant [$\text{mg} (\text{g min}^{1/2})^{-1}$].

In Fig. 2, it can be observed that multiple straight lines were obtained. Essentially, a multiple order process means that the process can be divided into two or three linear stages, where each stage would express a pseudo-first-order mechanism. The first stage is related to the initial binding of EtBr molecules on the active sites of Fe-CP and NP, and the other stages characterize a tendency of EtBr to form a constant layer on the adsorbent surface. It can be seen from Fig. 2 that the adsorption process during the first stage was much faster than during the other stages, which were controlled by a film or intraparticle diffusion mechanism [33]. In general, k_{ip} was found to increase while increasing the initial EtBr concentration which can be due to a greater concentration driving force [34].

3.3. Effect of adsorbent dose

The effect of the adsorbent dose on EtBr removal at a fixed pH (pH 10) and a fixed initial EtBr concentration (100 mg L^{-1}) is shown in Fig. 3. It was

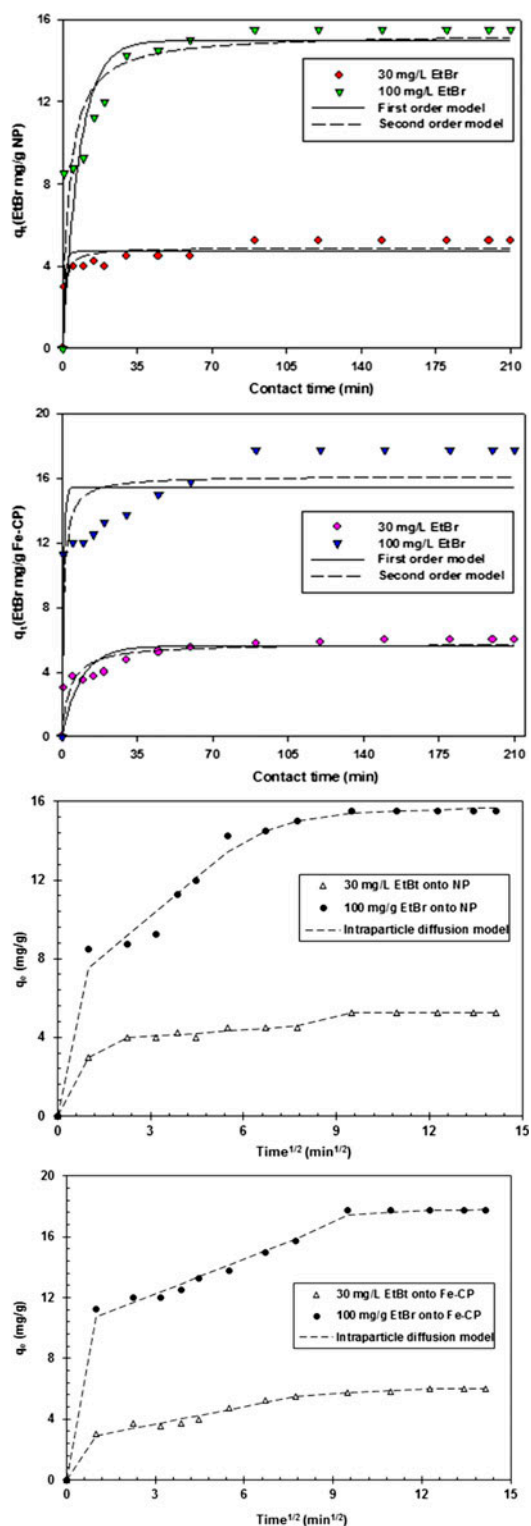


Fig. 2. Adsorption kinetics: pseudo-first-order, pseudo-second-order and intraparticle diffusion kinetics for adsorption isotherm of EtBr for NP and iron-coated pumice (Fe-CP).

evident that the percentage of EtBr removal increased with the increase of the adsorbent dose, which was due to a greater amount of adsorbent implies a greater number of available binding sites. The maximum adsorption capacity occurred using 10 g of adsorbents. However, it was also observed from Fig. 3 that, after an amount of 5 g L^{-1} , there was no significant change in the percentage removal of EtBr. This was most probably due to the overlapping of active sites at a higher adsorbent dose. Overlapping of active sites at a higher adsorbent dose could be a result of conglomeration of exchanger particles. Due to conglomeration of exchanger particles, there was not any appreciable increase in effective surface area, thereby keeping the percentage removal constant with any increase in adsorbent dose beyond these limits [35].

3.4. Effect of the initial pH on EtBr removal

Solution pH is an important factor controlling the surface charge of the adsorbent and the degree of ionization of the materials in the solution. To determine the optimum pH for maximum EtBr removal, the equilibrium adsorption of EtBr (for an initial concentration of 50 mg L^{-1}) was investigated for a pH range from 3 to 10, while the other parameters were maintained constants, namely 24°C and 4 g L^{-1} adsorbent dose. In Fig. 4, it is shown that the efficiency of removal increased with increasing pH for both adsorbents. As pH increased from 3 to 10, the removal efficiency of NP and Fe-CP for EtBr increased from 32.64 to 67.10% and from 46.04 to 70.98%, respectively. Maximum dye uptake was achieved at pH 10. High adsorption of EtBr at high pH indicated that the surface seems to be alkaline which decreases the protonation at their surfaces due to neutralization of positive charges, resulting in easier diffusion. At basic pH, since there is no electrostatic repulsion between the on-ionized EtBr species and the Fe-CP and NP, the adsorption is higher.

3.5. Adsorption isotherms

In this study, the experimental data of adsorption equilibrium were described by means of Langmuir and Freundlich isotherms, the most widely used ones. The Langmuir model is the simplest one, in which adsorption at any site is not influenced by neighboring sites, as may be the case with physical adsorption on a single layer. In its simplest form, only one type of species is available for adsorption. The Freundlich model is an empirical model for adsorbents in which

Table 3
Parameters of kinetic equations

Adsorbent	Conc. (mg L ⁻¹)	Pseudo-first-order model				Pseudo-second-order model			Intraparticle diffusion model	
		$q_{e,exp}$ (mg g ⁻¹)	$q_{e,cal}$ (mg g ⁻¹)	k_1	R^2	$q_{e,cal}$ (mg g ⁻¹)	k_2	R^2	k_{ip} (g mg ⁻¹ min ^{-1/2})	R^2
Fe-CP	30	6.005	5.610	0.110	0.852	5.777	0.047	0.918	0.390	0.850
	100	17.75	15.45	1.278	0.872	16.14	0.069	0.910	0.819	0.870
NP	30	5.250	4.718	0.969	0.929	4.905	0.221	0.957	0.157	0.889
	100	15.50	14.99	0.125	0.884	15.33	0.021	0.932	1.759	0.961

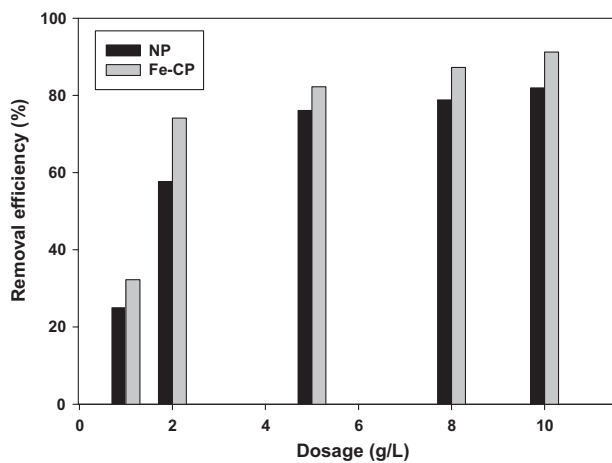


Fig. 3. Effect of adsorbent dose on EtBr removal (initial EtBr concentration = 100 mg L⁻¹; temperature 24 °C; pH 10; contact time 150 and 90 min for iron-coated pumice (Fe-CP) and NP, respectively).

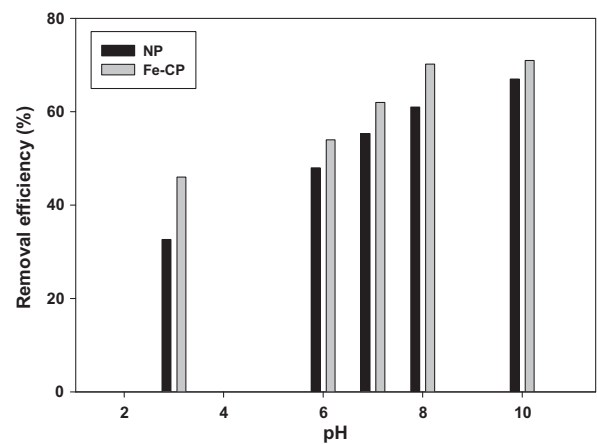


Fig. 4. Effect of solution pH on the adsorption of EtBr by iron-coated pumice (Fe-CP) and NP (Initial EtBr concentration = 50 mg L⁻¹; pH 10; adsorbent dose = 4 g L⁻¹; temperature = 24 °C and contact time 150 and 90 min for iron-coated pumice (Fe-CP) and NP, respectively).

the affinity of sites for adsorption is not uniform, i.e. where the sites with higher affinity will, statistically speaking, become occupied first. Langmuir isotherm can be used for physical adsorption in a single layer. The Langmuir isotherm can be expressed as follows [36]:

$$Q_e = \frac{q_m b C_e}{1 + b C_e} \quad (5)$$

where q_m is the maximum adsorption capacity and b is the Langmuir constant related to the energy of adsorption.

The Freundlich isotherm can be expressed as follows [37]:

$$q_e = K_F C_e^{1/n} \quad (6)$$

where K_F and $1/n$ are the Freundlich constants. For favorable adsorption, the value of n should be in the range from 1 to 10 [38]. In order to understand the adsorption type, equilibrium data were tested with the Dubinin-Radushkevich isotherm [39]. The linearized D-R equation can be written as follows:

$$\ln q_e = \ln q_m - K_{DR} \varepsilon^2 \quad (7)$$

where ε is the polanyi potential and is equal to $RT \ln(1 + 1/C_e)$, q_e is the amount of EtBr adsorbed per unit mass of adsorbents, q_m is the theoretical adsorption capacity, K_{DR} is the constant related to mean free energy, R is universal gas constant, and T is the absolute temperature (K). The mean free energy of adsorption (E) was calculated from the constant “ K ” using the relation [40]:

$$E_{DR} = (2K_{DR})^{-0.5} \quad (8)$$

E_{DR} is defined as the free energy change when 1 mol of ion is transferred to the surface of the solid from infinity in solution.

Isothermal studies of EtBr removal are shown in Fig. 5. The fit of experimental values using the three isotherm models was patterned and the results are presented in Table 4. As can be seen from the correlation coefficients (R^2), for both NP and Fe-CP, the Freundlich model fitted the experimental values better than the Langmuir model, indicating a heterogeneous surface binding. The Freundlich adsorption isotherm predicts that the pollutant (EtBr) concentrations on the adsorbents (Fe-CP and NP), i.e. adsorption capacity will increase if there is an increase in the EtBr concentration in the solution. The values of K_F and $1/n$ were calculated from the slope and intercept of the plot in Fig. 5 and they were reported in Table 4. K_F is a constant indicative of the adsorption capacity of the adsorbent; while n is an empirical constant related to the magnitude of the adsorption driving force [38]. It is shown from the results in Table 4 and Fig. 5 that the theoretical value of the adsorption capacity was higher for Fe-CP than NP, and this is probably due to the higher porosity of Fe-CP. However, the Langmuir constant, b , connected to the adsorption free energy and specifying the adsorbents affinity for EtBr binding, was higher for NP than Fe-CP, indicating a more favorable capability of EtBr molecules to form a stable complex with NP than with Fe-CP. The $1/n$ value from the Freundlich equation indicates that the relative distribution of energy sites depends on the nature and strength of the adsorption process. The value of

$1/n$ of adsorption EtBr onto Fe-CP surface was 0.762; indeed, this value refers to 76% of the active sites that have equivalent energy where adsorption happened. Furthermore, the values of $1/n$ closer to 1 indicate a homogeneous surface [41]. As observed, the Freundlich equation appeared to be the most suitable model to describe the experimental data. Thus, $R^2 = 0.997$ and $R^2 = 0.995$ were obtained for NP and Fe-CP, respectively. The fitting of the data to the Freundlich equation indicated the heterogeneity of the adsorbent surface. In addition, the n values of the Freundlich model for NP and Fe-CP were 1.311 and 1.312, respectively (Table 4), indicating strong interactions between the adsorbents and EtBr. The experimental results also showed that the interactions between Fe-CP and EtBr were higher than those of NP and EtBr. This is likely related to the higher porosity of Fe-CP stone, showing adsorption not only on the surface but also in its inner part. Comparing the q_m values obtained in this work with those of other adsorption studies [11,42,43], it can be seen that NP and Fe-CP have a high adsorption capacity. The plot of $\ln q_e$ against e^2 (not shown here) was almost linear with a correlation coefficient (R^2) of 0.951 and 0.805 for Fe-CP and NP, respectively. The value of q_m was 45.08 and 40.25 mg g^{-1} for Fe-CP and NP, respectively. In addition, the mean free energy, E_{DR} , evaluated using the D-R model was about 17.02 and 18.80 kJ mol^{-1} for NP and Fe-CP (Table 4), respectively, indicating that the adsorption of EtBr on NP and Fe-CP was a chemisorption process which occurred through ion exchange reactions [44].

3.6. Performance analysis of ANN training phases for NP and Fe-CP

The network architecture of 2-2-1 for analyzing A and B and 1-2-1 for analyzing C and D was found the best and optimal solution by having number of “trial and error” work. Network type is shown in Figs. 6–8. The input data are divided into 2 groups. The odd data points of A, B, C, D and removal capacities ($R\%$) were used for the training procedure, while the even data were used for the testing procedure. The following tables show the performance analysis of testing procedures for NP and Fe-CP. The maximum number of iterations was set to 15,000 during the training procedure. Therefore, the total training time is measured in just a few seconds. Following benchmark comparisons, an optimization was carried out for the best ANN algorithm. Then, the three-layer ANN was evaluated by the best training algorithm. Finally, the use of ANN based on tangential activation functions was investigated and compared with the classical

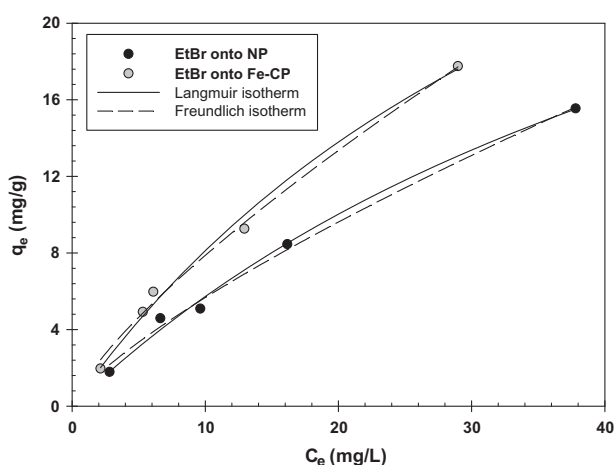


Fig. 5. Freundlich and Langmuir adsorption isotherms for EtBr adsorption onto NP and iron-coated pumice (Fe-CP).

Table 4
Isotherm constants for the adsorption of EtBr on NP and iron-coated pumice (Fe-CP)

Model	Parameters			
Freundlich isotherm	K_F (mg g ⁻¹)	n	R^2	
	Fe-CP	1.360	1.311	0.997
	NP	0.982	1.312	0.995
Langmuir isotherm	q_{max} (mg g ⁻¹)	b (L mg ⁻¹)	R^2	
	Fe-CP	45.80	0.021	0.987
	NP	40.25	0.016	0.988
Dubinin-Radushkevich isotherm	q_m (mg g ⁻¹)	E_{DR} (kJ mol ⁻¹)	R^2	
	Fe-CP	14.51	18.83	0.951
	NP	10.10	17.02	0.805

Table 5
Performance analysis of training procedures for NP and iron-coated pumice (Fe-CP)

Analyzed factors	Std. dev	Max. error	Correlation	RMS error
A and B (for NP)	0.795	1.692	0.9993	0.0080
C (for NP)	0.534	0.798	0.9983	0.0155
D (for NP)	1.061	1.341	0.9991	0.0130
A and B (for Fe-CP)	1.338	2.791	0.9989	0.0105
C (for Fe-CP)	6.349	9.436	0.9561	0.0809
D (for Fe-CP)	0.206	0.216	0.9998	0.0050

Note: A: concentration, B: time, C: pH, D: dose, std. dev: standard deviation.

Table 6
The real and estimated values of removal efficiencies for concentration and time using NP and iron-coated pumice (Fe-CP)

NP		Fe-CP	
Real	Estimated	Real	Estimated
40	37.68	40	32.80
53	53.17	47	42.60
53	53.99	53	52.19
60	60.89	70	70.87
70	67.88	78	80.73
70	69.33	89	86.76
70	70.23	89	89.32

feed-forward back-propagation neural networks. Therefore, the proposed technique is simple to implement and requires less computational time. One of the aims in modeling the experimental system is to decide the optimal parameters. In order to obtaining the optimal parameters, an optimization algorithm should be employed. The optimization algorithm needs the selection of those parameters, and its associated values are

Table 7
The real and estimated values of pH using NP and iron-coated pumice (Fe-CP)

NP		Fe-CP	
Real	Estimated	Real	Estimated
80.6	80.80	69.3	46.61
75.3	74.48	34.6	41.02
67.0	63.63	60.0	61.77

Table 8
The real and estimated values of dose using NP and iron-coated pumice (Fe-CP)

NP		Fe-CP	
Real	Estimated	Real	Estimated
46.3	40.28	8.99	7.599
78.8	82.12	31.1	28.45

most important for removal efficiency. In order to achieve this, the analyzed parameters should be at a

Table 9

Optimized values for analyzed factors for NP and iron-coated pumice (Fe-CP)

NP		Fe-CP	
A	9	A	22.72
B	154 min	B	210 min
C	2 mg L ⁻¹	C	2 mg L ⁻¹
D	8 mg g ⁻¹	D	10 mg g ⁻¹

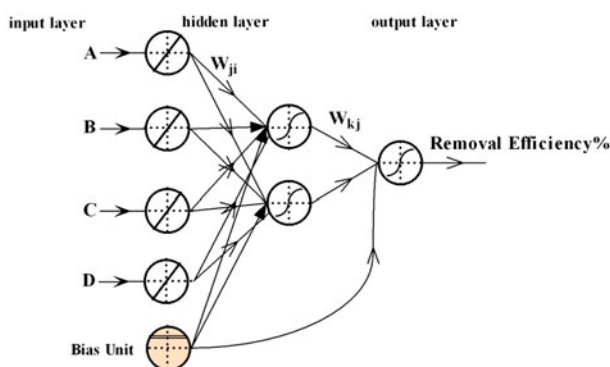


Fig. 6. Network type for modeling the experimental system.

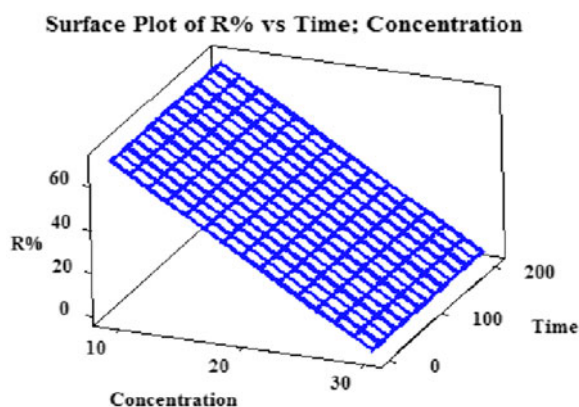


Fig. 7. Removal efficiency with respect to A and B using NP.

minimum when the removal efficiency is at maximum. Generally, simplex algorithm is used for optimization purposes. In our study, using the optimization algorithm to maximize the removal efficiency, the analyzed parameters were chosen (Tables 5–9).

Surface Plot of R% vs Time; Concentration

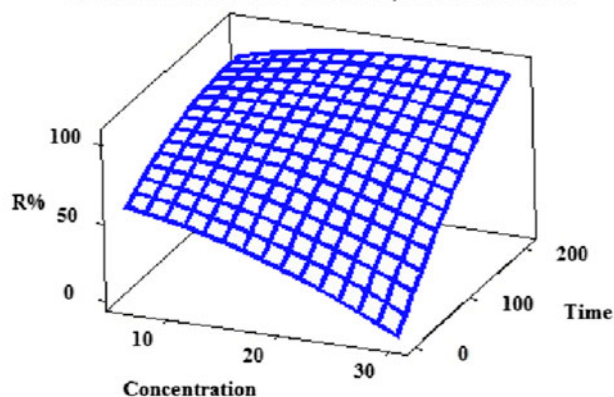


Fig. 8. Removal efficiency with respect to A and B using iron-coated pumice (Fe-CP).

4. Conclusions

Fe-CP and NP were investigated for the removal of EtBr from aqueous solutions. Experimental results showed that Fe-CP has a greater capacity to adsorb EtBr than NP. Adsorption equilibrium was reached within 90 and 150 min for NP and Fe-CP, respectively. Adsorption processes for the EtBr were found to follow the pseudo-second-order kinetics model. Regarding adsorption isotherms, the Freundlich model fitted the experimental data more accurately than the Langmuir one. Maximum adsorption capacity (q_m) was found to be 40.25 and 45.08 mg g⁻¹ for NP and Fe-CP, respectively. The results showed that EtBr removal increased with contact time and in basic conditions. A feed-forward neural network was proposed to predict the removal of EtBr from aqueous solutions by NP and Fe-CP taking into account the effect of initial pH, contact time, initial EtBr concentration, and adsorbent dose. A simple back-propagation feed-forward network with three hidden layers consisting of 2–2–1 and 1–2–1 neurons in each layer was proposed. The minimum mean square error was found to be 0.005, with a 99.98% correlation.

Acknowledgments

The authors would like to thank Dr J. (Jos) Laven from the Department of Chemical Engineering and Chemistry, Materials and interface Chemistry, Technische Universiteit Eindhoven, Eindhoven, Netherlands, for their helpful suggestions in the modification methods. Also, authors are thankful to the Student Research Committee, Mazandaran University of Medical Sciences, Sari, Iran, for the financial support under project grant 93-78.

References

- [1] R.K. Gupta, R. Pandey, G. Sharma, R. Prasad, B. Koch, S. Srikrishna, P.-Z. Li, Q. Xu, D.S. Pandey, DNA binding and anti-cancer activity of redox-active heteroleptic piano-stool Ru(II), Rh(III), and Ir(III) complexes containing 4-(2-methoxyppyridyl)phenyldipyrrromethene, *Inorg. Chem.* 52 (2013) 3687–3698.
- [2] C. Zhang, L. Liu, J. Wang, F. Rong, D. Fu, Electrochemical degradation of ethidium bromide using boron-doped diamond electrode, *Sep. Purif. Technol.* 107 (2013) 91–101.
- [3] P. Quillardet, M. Hofnung, Ethidium bromide and safety—Readers suggest alternative solutions, *Trends Genet.* 4 (1988) 89–90.
- [4] J. Carbajo, C. Adán, A. Rey, A. Martínez-Arias, A. Bahamonde, Optimization of H₂O₂ use during the photocatalytic degradation of ethidium bromide with TiO₂ and iron-doped TiO₂ catalysts, *Appl. Catal. B: Environ.* 102 (2011) 85–93.
- [5] C. Adán, A. Martínez-Arias, M. Fernández-García, A. Bahamonde, Photocatalytic degradation of ethidium bromide over titania in aqueous solutions, *Appl. Catal. B: Environ.* 76 (2007) 395–402.
- [6] M. Khraisheh, L. Wu, A.a.H. Al-Muhtaseb, A.B. Albadarin, G.M. Walker, Phenol degradation by powdered metal ion modified titanium dioxide photocatalysts, *Chem. Eng. J.* 213 (2012) 125–134.
- [7] J. Galán, A. Rodríguez, J.M. Gómez, S.J. Allen, G.M. Walker, Reactive dye adsorption onto a novel mesoporous carbon, *Chem. Eng. J.* 219 (2013) 62–68.
- [8] A.H. Al-Muhtaseb, K.A. Ibrahim, A.B. Albadarin, O. Ali-khashman, G.M. Walker, M.N.M. Ahmad, Remediation of phenol-contaminated water by adsorption using poly(methyl methacrylate) (PMMA), *Chem. Eng. J.* 168 (2011) 691–699.
- [9] F. Najafi, M. Norouzi, K. Zare, A. Fakhri, Removal of ethidium bromide by carbon nanotube in aqueous solution: Isotherms, equilibrium mechanism studies, and its comparison with nanoscale of zero valent iron as adsorbent, *J. Nanostruct. Chem.* 3 (2013) 60–66.
- [10] M.W. Oliveira, A.W.S. Hilsdorf, A. Silva, A.F. Oliveira, Study of ethidium bromide adsorption on XAD-7 resin, *Química Nova* 32 (2014) 1134–1138.
- [11] O. Moradi, A. Fakhri, S. Adami, S. Adami, Isotherm, thermodynamic, kinetics, and adsorption mechanism studies of ethidium bromide by single-walled carbon nanotube and carboxylate group functionalized single-walled carbon nanotube, *J. Colloid Interface Sci.* 395 (2013) 224–229.
- [12] L.B. Far, B. Souri, M. Heidari, R. Khoshnavazi, Evaluation of iron and manganese-coated pumice application for the removal of as(V) from aqueous solution, *Iran. J. Environ. Health Sci. Eng.* 9 (2012) 1–9.
- [13] B. Heibati, S. Rodriguez-Couto, A. Amrane, M. Rafatullah, A. Hawari, M.A. Al-Ghouti, Uptake of Reactive Black 5 by pumice and walnut activated carbon: Chemistry and adsorption mechanisms, *J. Ind. Eng. Chem.* 20 (2014) 2939–2947.
- [14] M. Kitis, E. Karakaya, N.O. Yigit, G. Civelekoglu, A. Akcil, Heterogeneous catalytic degradation of cyanide using copper-impregnated pumice and hydrogen peroxide, *Water Res.* 39 (2005) 1652–1662.
- [15] A.H. Mahvi, B. Heibati, A. Mesdaghinia, Fluoride adsorption by pumice from aqueous solutions, *E-J. Chem.* 9 (2012) 1843–1853.
- [16] A.H. Mahvi, B. Heibati, Removal of Reactive Red 120 and Direct Red 81 dyes from aqueous solutions by pumice, *Res. J. Chem. Environ.* 16 (2012) 64–68.
- [17] F. Akbal, Sorption of phenol and 4-chlorophenol onto pumice treated with cationic surfactant, *J. Environ. Manage.* 74 (2005) 239–244.
- [18] N. Moraci, P.S. Calabrò, Heavy metals removal and hydraulic performance in zero-valent iron/pumice permeable reactive barriers, *J. Environ. Manage.* 91 (2010) 2336–2341.
- [19] B. Ozturk, Y. Yildirim, Investigation of sorption capacity of pumice for SO₂ capture, *Proc. Saf. Environ. Prot.* 86 (2008) 31–36.
- [20] M. Kitis, S.S. Kaplan, E. Karakaya, N.O. Yigit, G. Civelekoglu, Adsorption of natural organic matter from waters by iron coated pumice, *Chemosphere* 66 (2007) 130–138.
- [21] F. Moattar, S. Naseri, M.T. Samadi, N. Khorasani, Evaluation of aluminum-coated pumice as a potential arsenic(V) adsorbent from water resources, *Int. J. Environ. Res.* 5 (2011) 447–456.
- [22] N.G. Turan, B. Mesci, O. Ozgonenel, Artificial neural network (ANN) approach for modeling Zn(II) adsorption from leachate using a new biosorbent, *Chem. Eng. J.* 173 (2011) 98–105.
- [23] K. Yetilmmezsoy, S. Demirel, Artificial neural network (ANN) approach for modeling of Pb(II) adsorption from aqueous solution by Antep pistachio (*Pistacia vera* L.) shells, *J. Hazard. Mater.* 153 (2008) 1288–1300.
- [24] N. Daneshvar, A.R. Khataee, N. Djafarzadeh, The use of artificial neural networks (ANN) for modeling of decolorization of textile dye solution containing C. I Basic Yellow 28 by electrocoagulation process, *J. Hazard. Mater.* 137 (2006) 1788–1795.
- [25] N. Prakash, S.A. Manikandan, L. Govindarajan, V. Vijayagopal, Prediction of biosorption efficiency for the removal of copper(II) using artificial neural networks, *J. Hazard. Mater.* 152 (2008) 1268–1275.
- [26] L. Yingwei, N. Sundararajan, P. Saratchandran, Performance evaluation of a sequential minimal radial basis function (RBF) neural network learning algorithm, *Neural Net., IEEE Trans.* 9 (1998) 308–318.
- [27] M.N. Sepehr, V. Sivasankar, M. Zarrabi, M. Senthil Kumar, Surface modification of pumice enhancing its fluoride adsorption capacity: An insight into kinetic and thermodynamic studies, *Chem. Eng. J.* 228 (2013) 192–204.
- [28] A. APHA, WEF, standard Methods for the Examination of Water and Wastewater, twentieth ed., American Public Health Association, Washington, DC, 2005.
- [29] Y. Glocheux, M. Pasarín, A.B. Albadarin, S.J. Allen, G.M. Walker, Removal of arsenic from groundwater by adsorption onto an acidified laterite by-product, *Chem. Eng. J.* 228 (2013) 565–574.
- [30] Y.S. Ho, G. McKay, Pseudo-second order model for sorption processes, *Process Biochem.* 34 (1999) 451–465.
- [31] S. Lagergren, Zur theorie der sogenannten adsorption gelöster stoffe (About the theory of so-called adsorption of soluble substances), *Kungliga Svenska Vetenskapsakademiens Handlingar* 24 (1898) 1–39.

- [32] W.J. Weber, J.C. Morris, Kinetics of adsorption on carbon from solution, *J. Sanitary Eng. Div.: Am. Soc. Civ. Eng.* 89 (1963) 31–59.
- [33] A.B. Albadarin, C. Mangwandi, G.M. Walker, S.J. Allen, M.N. Ahmad, Biosorption characteristics of sawdust for the removal of Cd(II) Ions: Mechanism and thermodynamic studies, *Chem. Eng. Trans.* 24 (2011) 1297–1302.
- [34] A.B. Albadarin, C. Mangwandi, A.a.H. Al-Muhtaseb, G.M. Walker, S.J. Allen, M.N.M. Ahmad, Kinetic and thermodynamics of chromium ions adsorption onto low-cost dolomite adsorbent, *Chem. Eng. J.* 179 (2012) 193–202.
- [35] P. Janos, H. Buchtová, M. Rýznarová, Sorption of dyes from aqueous solutions onto fly ash, *Water Res.* 37 (2003) 4938–4944.
- [36] I. Langmuir, The adsorption of gases on plane surfaces of glass, mica and platinum, *J. Am. Chem. Soc.* 40 (1918) 1361–1403.
- [37] H.M.F. Freundlich, Over the adsorption in solution, *J. Phys. Chem.* 57 (1906) 385–471.
- [38] D. Mohan, K.P. Singh, Single and multi-component adsorption of cadmium and zinc using activated carbon derived from bagasse—An agricultural waste, *Water Res.* 36 (2002) 2304–2318.
- [39] M. Doğan, M. Alkan, Ö. Demirbaş, Y. Özdemir, C. Özmetin, Adsorption kinetics of maxilon blue GRL onto sepiolite from aqueous solutions, *Chem. Eng. J.* 124 (2006) 89–101.
- [40] M.-S. Chiou, G.-S. Chuang, Competitive adsorption of dye metanil yellow and RB15 in acid solutions on chemically cross-linked chitosan beads, *Chemosphere* 62 (2006) 731–740.
- [41] B. Heibati, S. Rodriguez-Couto, M.A. Al-Ghouti, M. Asif, I. Tyagi, S. Agarwal, V.K. Gupta, Kinetics and thermodynamics of enhanced adsorption of the dye AR 18 using activated carbons prepared from walnut and poplar woods, *J. Mol. Liq.* 208 (2015) 99–105.
- [42] M. Demir, O. Gulnaz, Removal of ethidium bromide from aqueous solution by using Photomogetom crispus, *J. Biotechnol.* 185(Suppl.) (2014) S61–S62.
- [43] A. Fakhri, Assessment of ethidium bromide and ethidium monoazide bromide removal from aqueous matrices by adsorption on cupric oxide nanoparticles, *Ecotoxicol. Environ. Saf.* 104 (2014) 386–392.
- [44] A.B. Albadarin, J. Mo, Y. Glocheux, S. Allen, G. Walker, C. Mangwandi, Preliminary investigation of mixed adsorbents for the removal of copper and methylene blue from aqueous solutions, *Chem. Eng. J.* 255 (2014) 525–534.